Disease Models & Mechanisms 6, 489-502 (2013) doi:10.1242/dmm.010884

A patient-derived stem cell model of hereditary spastic paraplegia with *SPAST* mutations

Greger Abrahamsen[1,*], Yongjun Fan[1,*], Nicholas Matigian[1], Gautam Wali[1], Bernadette Bellette[1], Ratneswary Sutharsan[1], Jyothy Raju[1], Stephen A. Wood[1], David Veivers[2], Carolyn M. Sue[2] and Alan Mackay-Sim[1,‡]

SUMMARY

Hereditary spastic paraplegia (HSP) leads to progressive gait disturbances with lower limb muscle weakness and spasticity. Mutations in *SPAST* are a major cause of adult-onset, autosomal-dominant HSP. Spastin, the protein encoded by *SPAST*, is a microtubule-severing protein that is enriched in the distal axon of corticospinal motor neurons, which degenerate in HSP patients. Animal and cell models have identified functions of spastin and mutated spastin but these models lack the gene dosage, mutation variability and genetic background that characterize patients with the disease. In this study, this genetic variability is encompassed by comparing neural progenitor cells derived from biopsies of the olfactory mucosa from healthy controls with similar cells from HSP patients with *SPAST* mutations, in order to identify cell functions altered in HSP. Patient-derived cells were similar to control-derived cells in proliferation and multiple metabolic functions but had major dysregulation of gene expression, with 57% of all mRNA transcripts affected, including many associated with microtubule dynamics. Compared to control cells, patient-derived cells had 50% spastin, 50% acetylated α-tubulin and 150% stathmin, a microtubule-destabilizing enzyme. Patient-derived cells were smaller than control cells. They had altered intracellular distributions of peroxisomes and mitochondria and they had slower moving peroxisomes. These results suggest that patient-derived cells might compensate for reduced spastin, but their increased stathmin expression reduced stabilized microtubules and altered organelle trafficking. Sub-nanomolar concentrations of the microtubule-binding drugs, paclitaxel and vinblastine, increased acetylated α-tubulin levels in patient cells to control levels, indicating the utility of this cell model for screening other candidate compounds for drug therapies.

INTRODUCTION

Hereditary spastic paraplegia (HSP) is a genetically heterogeneous group of disorders that commonly affect the long fibers of the corticospinal tract and posterior columns in the spinal cord, leading to progressive gait disturbances with muscle weakness and spasticity (Salinas et al., 2008). More than 40 gene loci are associated with HSP, which may be autosomal dominant, recessive or X-linked recessive. Mutations in *SPG4/SPAST* account for the largest group of adult-onset HSP cases and about 40-44% of all autosomal-dominant 'uncomplicated' HSP (i.e. without other signs such as ataxia, dementia or retardation) (Salinas et al., 2008; Vandebona et al., 2012). Spastin, the protein encoded by *SPAST*, is a member of the AAA (ATPases associated with diverse cellular activities) group of proteins, which are involved in cell cycle regulation, protein degradation, organelle biogenesis and vesicle-mediated functions (Roll-Mecak and McNally, 2010). Spastin is involved with microtubule disassembly (Errico et al., 2002) and is enriched in the distal axon of corticospinal motor neurons (reviewed in Salinas et al., 2007), the degeneration of which is seen post-mortem in the spinal cords of HSP patients, histologically (Deluca et al., 2004) and after magnetic imaging (Hedera et al., 2005). The cellular mechanisms whereby *SPAST* mutations cause axon degeneration are not understood but spastin mutations cause disrupted axonal transport (McDermott et al., 2003; Molon et al., 2004). Consistent with these findings, *Spg4* mutant mice had gait abnormalities, axonal swellings in cortical axons *in vitro* and reduced anterograde axonal transport of mitochondria and β-amyloid precursor protein (APP)-containing membrane bound organelles (Kasher et al., 2009). Overexpression of mutated *SPAST* in HEK293 cells led to increased perinuclear distribution of mitochondria and peroxisomes (McDermott et al., 2003).

Until now, functions of spastin and mutated spastin have been identified *in vitro*, by over- or underexpression in human and animal cell lines, and in genetically modified mouse and *Drosophila* models. Although instructive, these models lack the gene dosage, mutation variability and genetic background that characterize patients with the disease and that presumably underlie the variable clinical outcome. Central questions remain concerning the cellular consequences of *SPAST* mutations and how these cause an adult-onset disease, with variable severity and age of onset, affecting mainly the long axons of the corticospinal tract.

To address these issues, we developed a new patient-derived stem cell model for HSP, based on neural progenitors from the organ of smell in the nose. These cells are generated from biopsies of olfactory mucosa (Féron et al., 1998) grown in defined medium to produce multipotent neural progenitors (Murrell et al., 2005) and then propagated as adherent cultures (olfactory neurosphere-derived, ONS, cells) (Matigian et al., 2010). ONS cells are standardized cell populations grown under strict quality assurance such that technical

[1]National Centre for Adult Stem Cell Research, Eskitis Institute for Cell and Molecular Therapies, Griffith University, Brisbane, Queensland 4111, Australia
[2]Kolling Institute of Medical Research, University of Sydney, Sydney, New South Wales 2065, Australia
*These authors contributed equally to this work
‡Author for correspondence (a.mackay-sim@griffith.edu.au)

Received 17 September 2012; Accepted 29 November 2012

TRANSLATIONAL IMPACT

Clinical issue

Hereditary spastic paraplegia (HSP) is a neurodegenerative disease affecting children and adults, and causes weakness and spasticity of the lower limbs. The disease progressively worsens throughout life, eventually leading to paralysis. HSP is a hereditary disease caused by mutation in any of more than 40 genes, and is characterized by variable age of onset and severity, thought to be due to differences in genetic background. The absence of treatments means that there is a pressing need to understand how different mutations cause HSP and to find new therapies. Mutations in *SPAST*, which codes for a microtubule-destabilizing protein called spastin, cause adult-onset HSP. The functions of spastin and mutated spastin have been described using genetically manipulated cell lines, fly and mouse models. Patient-derived cells are a more disease-relevant model because they embody the variable genetic background of the human population.

Results

In this paper, the authors present a new patient-cell-based model for investigating HSP using the stem cells from the sense organ of smell in the nose, which continually regenerate the olfactory sensory neurons throughout adult life. Compared with cells from healthy controls, cells from patients with HSP had 50% of the amount of spastin, in line with the presence of one normal and one mutated copy of *SPAST* in patient cells. This was associated with a change in the expression of 57% of the genes in patient cells, including many genes associated with microtubule functions, which were significantly altered in patient cells. Marked microtubule degeneration is seen in the spinal cord of HSP patients. Cells from patients have less acetylated α-tubulin, a marker of stable microtubules, which can be explained by the higher levels of stathmin, a microtubule-associated protein whose function is similar to spastin; stathmin also destabilizes microtubules. Patient cells showed altered intracellular distributions of peroxisomes and mitochondria (organelles that depend on microtubules for their trafficking throughout the cell), and trafficking speed was slower in patient cells. Finally, the authors demonstrate that very low doses of microtubule-binding drugs can restore the levels of acetylated α-tubulin in patient cells to those found in control cells.

Implications and future directions

This study provides a baseline of genetic, protein and functional analyses using patient-derived neural stem cells carrying *SPAST* mutations. This model can be applied to patient-derived cells bearing other mutations. The model also provides a robust platform for the discoveries of new drug therapies.

variables are small compared with individual patient and donor variability (Mar et al., 2011; Matigian et al., 2010). This model has revealed novel and significant alterations in disease-specific cell functions in schizophrenia and sporadic Parkinson's disease, two diseases of unknown genetics (Cook et al., 2011; Fan et al., 2012; Mackay-Sim, 2012; Mar et al., 2011; Matigian et al., 2010). In the present study, we investigated the functional consequences of *SPAST* mutations in ONS cells derived from patients with adult-onset HSP but with a variety of *SPAST* mutations, with the aim of identifying common molecular mechanisms affecting cellular functions.

When ONS cells from nine patients and ten healthy controls were compared for gene and protein expression and for a variety of cell functions, it was apparent that patient-derived cells were in a state of homeostatic compensation for their reduced spastin. Although this maintained many cell functions within the normal range, it was associated with overexpression of stathmin (a microtubule-destabilizing enzyme), reduced cell size, reduced stabilized microtubules, altered intracellular distributions of peroxisomes and mitochondria, and reduced speed of peroxisome movement.

RESULTS

We compared cells from patients ('patient cells') and those from healthy controls ('control cells') using flow cytometry, gene expression profiling, protein expression analysis and cell function analyses that included assays of cell proliferation, metabolic function and cell morphometry to quantify content and distribution of intracellular organelles. The *SPAST* mutations carried by the patients included missense, exon-skipping, nonsense and exonic deletion affecting seven different exons (Table 1). All patient cells had similar gene and protein expression, and similar cell functions, with no outliers related to the type of *SPAST* mutation.

Patient and control cells had similar immunophenotype, proliferation and metabolism

Patient and control cells were grown as neurospheres (Fig. 1A) and then dissociated and grown in adherent cultures (Fig. 1B). Flow cytometric analysis showed a similar immunophenotype for cells from patients and controls (Fig. 1C,D). Similar proportions of patient and control cells expressed mesenchymal stem cell markers (CD105, CD73), neural stem/progenitor markers (NES, TUBB3, GFAP) and embryonic stem cell marker (OCT4), with little or no expression of CD45 or SOX2 (Fig. 1D). Analysis of variance found no significant difference in expression of these markers between patient and control cells ($F_{1,117}$=0.40).

Patient and control cells did not differ in cell proliferation rates over a 72-hour period *in vitro* (Fig. 1E; $F_{1,51}$=0.02). The metabolic functions of the patient and control cells were also similar. There were no significant differences between patient and control cells across six different metabolic functions tests for oxidative state, apoptosis, proteasome function and mitochondrial function (Fig. 1F; $F_{1,136}$=2.45).

Patient cells had significantly dysregulated gene expression

Of the 24,526 probes on the arrays, 10,000 were detected (patient cells, n=9542; control cells, n=9472). Gene expression levels of the patient cells were compared with the control cells, revealing that patient cells differentially expressed 57% of the detected genes (5723/10,000, P<0.01, Benjamini and Hochberg false discovery rate correction) (supplementary material Table S1). Of the differentially expressed genes, 1229 (13% of detected genes) were twofold increased or decreased in patient cells compared with controls (supplementary material Table S1). Raw microarray data are available in the ArrayExpress database (http://www.ebi.ac.uk/arrayexpress) under accession number (E-TABM-1180).

Unsupervised cluster analysis was used to test the degree of similarity between the gene expression levels of the samples, based on the total detected genes with the criterion that all included genes were present in 50% of samples in either group. This analysis clearly separated the patient cells from the control cells, demonstrating the strong similarity in gene expression within each group and the differences in gene expression between groups (Fig. 1G). Principal components analysis on the differentially expressed genes similarly separated the patient cells from the control cells, while showing clear differences between them (supplementary material Fig. S1). The primary component, accounting for 34% of variance in gene expression, separated patient and control cells into two groups. The secondary component, accounting for a further 19% of the variance, separated individuals in patient and control groups across a similar

Table 1. Patient and control participants

Cell line ID	Short ID	Sex	Age at biopsy	Mutation	Exon/intron
HSP patients with *SPAST* mutations					
610070001	H701	M	64	c.1413+3_1413+6del	Intron 11
610080001	H801	F	46	p.E464D; c.1392 A>T	Exon 11
610080002	H802	F	50	p.L195V; c.583C>G	Exon 3
610080003	H803	M	51	p.L195V; c.583C>G	Exon 3
610080006	H806	M	57	p.E366K; c.1096G>A	Exon 7
610090001	H901	M	71	p.W148X; c.444G>A	Exon 2
610090002	H902	F	42	p.S597G; c.1789 A>G	Exon 17
610090003	H903	M	24	p.S597G; c.1789 A>G	Exon 17
610090004	H904	M	35	ex8-9del	Exon 8-9
Controls					
100080001	C801	F	55	–	–
100080002	C802	M	59	–	–
100080003	C803	F	66	–	–
100080004	C804	F	59	–	–
100080008	C808	M	61	–	–
100080013	C813	M	64	–	–
100080015	C815	F	64	–	–
100080016	C816	M	60	–	–
100080017	C817	M	49	–	–
100090001	C901	F	70	–	–

Mutation analysis of the patients was reported previously (Vandebona et al., 2012).

range, with no obvious association with the type of mutation in the patient cells.

Considering the known role of spastin in microtubule severing, it was of interest that the gene ontology (GO) analysis identified microtubule functions to be significantly over-represented in patient cells. Taking the more stringently defined list of differentially expressed genes, of the genes ascribed to microtubule function, 46 were present in the 1229 genes that were twofold differentially expressed (Table 2, P=7.26E-08). When considering the total 5723 differentially expressed genes, 118/298 microtubule function genes were over-represented (P=4.6E-06, supplementary material Table S2). At the individual gene level, it is notable that *STMN1*, coding for stathmin, a microtubule-severing protein, is common to most of the microtubule-associated functions (Table 2). *STMN1* was overexpressed in patient cells as were as 12 kinesins (*KIFs*) and eight tubulins (*TUBs*), with three kinesins and two tubulins downregulated (supplementary material Table S3).

There was no patient-control difference in *SPAST* mRNA expression although the expression of *SPG3A* (the gene for atlastin and binding partner of spastin) was significantly overexpressed. *SPG3A* and *STMN1* expression levels were confirmed independently (*SPG3A*, array, 2.3-fold, P<0.001; qRT-PCR, 1.9-fold, P<0.01; *STMN1*, array, 6.6-fold, P<0.001; qRT-PCR, 2.6-fold, P<0.0001). Overexpression of *KATNB1*, the gene for the microtubule severing protein, katanin-p80, was also confirmed (array, 1.3, P<0.001; qRT-PCR, 1.5-fold, P<0.0001). Associated genes (*KATNA1, KATNAL2*) were underexpressed on the array but were not different by qPCR, whereas *KATNAL1*, not present on the array, was significantly overexpressed (qRT-PCR, 2.1-fold, P<0.01).

Patient cells expressed less spastin protein

Both isoforms of spastin were expressed in patient and control cells. Patient cells expressed less of both isoforms compared with control cells (Fig. 2A,B). Analysis of variance indicated that patient cells expressed significantly less spastin than control cells ($F_{1,34}$=26.11, P<0.0001). The data are replotted in Fig. 2C, with the patient cell isoform content normalized against the control cell content for the same isoform, showing clearly the 50% reduction in both isoforms in patient cells. Post-hoc Bonferroni tests indicated that the patient cells expressed significantly less of each isoform (large, t=3.16, P<0.01; small, t=3.67, P<0.01).

Patient cells expressed more stathmin protein

The expression of several microtubule-related proteins was measured by western blot analysis (Fig. 3; supplementary material Fig. S2). The mean level of atlastin was higher in patient cells but the difference was not significant (t=1.07, d.f.=17, P=0.30), nor was the mean level of katanin-p80 significantly different (t=1.37, d.f.=17, P=0.27). The mean level of stathmin was raised significantly in patient cells by 50% (t=2.22, d.f.=17, P=0.04) whereas there was no difference in phosphorylated stathmin (t=0.04, d.f.=17, P=0.97).

Patient cells expressed less acetylated α-tubulin protein

The expression of post-translationally modified forms of α-tubulin was measured as an indicator of microtubule dynamics (Fig. 3; supplementary material Figs S3, S4). The mean level of detyrosinated α-tubulin was higher in patient cells but the difference was not significant (t=1.60, d.f.=17, P=0.13), nor was the mean level of tyrosinated α-tubulin significantly different (t=0.26, d.f.=17, P=0.80). The mean level of acetylated α-tubulin was reduced to

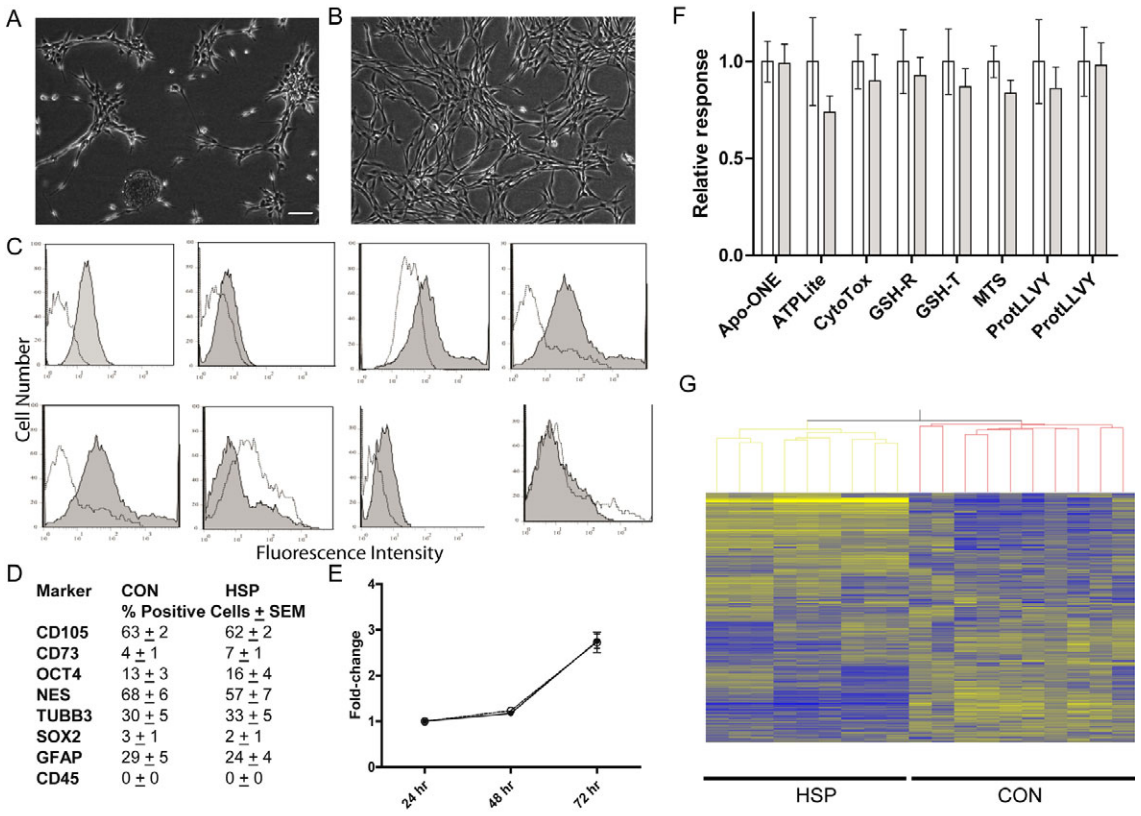

Fig. 1. Patient and control ONS cells had very large differences in gene expression. (A) Example of neurospheres forming *in vitro* in serum-free medium containing EGF and FGF2. (B) Examples of adherent ONS cells after passage of dissociated neurospheres, in serum-containing medium. Scale bar: 100 µm. (C) Examples of flow cytometric plots quantifying the numbers of cells (*y*-axis) against fluorescence intensity for each cell (*x*-axis) for each of the antigens indicated. Shaded curve shows cells labeled with an antibody to the antigen indicated. Open curve shows cells labeled with an isotype control antibody. (D) Positive cells calculated as the mean percentage of antibody-labeled cells with fluorescence intensity greater than the most fluorescent isotype control (n=9 or 10). (E) Rates of proliferation of patient cells (dashed line) and control cells (continuous line), expressed as a fold-change from the number at 24 hours (*y*-axis). (F) Responses of patient and control ONS cells in eight cell function assays: patient (shaded bars) and control (open bars). The response of each ONS cell line is normalized against the mean of the control cells for each assay (n=10). (G) Unsupervised cluster analysis of differentially expressed genes sorts the ONS cells into patients and controls. Rows are genes. Columns are individuals. The level of gene expression is indicated by the tone of the lines from overexpressed (yellow) to underexpressed (blue). Data in D-F indicate mean ± s.e.m.

50%; this difference between patients and controls was significant (t=2.71, d.f.=17, P=0.01).

The expression of acetylated α-tubulin was then quantified from the intensity of fluorescence of immunostained patient and control cells using automated image analysis (Fig. 4). The fluorescence intensity of acetylated α-tubulin immunoreactivity in the cytoplasm of at least 3000 individual cells in each control and patient cell line provided a mean fluorescence for each cell line. Individual means were averaged across all cell lines in each group. This experiment and analysis were performed in two independent experiments with different aliquots of cells and the data pooled for analysis. In order to control for overall fluorescence intensity variation between experiments, the fluorescence intensity for each cell line was expressed as a proportion of the mean intensity for the control group for each experiment, to give a relative intensity measurement, expressed as a percentage. This analysis confirmed that acetylated α-tubulin expression was significantly less in patient cells than in control cells (t=4.87, d.f.=36; control, 100% ± 2.5; patient, 78% ± 3.7, P<0.0001).

Patient cells had altered distributions of microtubules, mitochondria and peroxisomes

By visual inspection there was no obvious difference in the morphology of patient and control cells (supplementary material Figs S5, S6) but these became evident after image analysis. There were significant disease-related differences in the intracellular distribution of acetylated α-tubulin immunoreactivity, mitochondrial fluorescence and peroxisome density (Fig. 4).

The fluorescence intensity of acetylated α-tubulin immunoreactivity was quantified within three defined intracellular regions using automated image analysis: close to the nucleus (inner region), close to the cell membrane (outer region) and between these (middle region). Two-way ANOVA was performed with disease status and region as main effects. Acetylated α-tubulin immunoreactivity in patient cells was significantly different from that in control cells (disease status, $F_{1,51}$=48.18, P<0.0001) with significant differences in distributions between the regions (region, $F_{1,51}$=172.40, P<0.0001). Post-hoc Bonferroni adjusted t-tests showed that acetylated α-tubulin

Table 2. Microtubule-associated gene ontology functions of differentially expressed genes

Gene ontology function	Total genes* (*n*)	Differentially expressed genes		Genes†
		n	% GO function	
Formation of microtubules	57	11	19	*BIRC5*, *CDC25B*, *CENPF*, *CLIP1*, *DLGAP5*, *FES*, *FKBP4*, *FOXM1*, *NUSAP1*, *PSRC1*, ***STMN1***
Polymerization of microtubules	34	8	24	*CENPF*, *CLIP1*, *DLGAP5*, *FES*, *FKBP4*, *FOXM1*, *PSRC1*, ***STMN1***
Stabilization of microtubules	83	7	8	*BIRC5*, *DCLK1*, *DCLK2*, *KIFC1*, *MBP*, *NQO1*, ***STMN1***
Bundling of microtubules	20	6	30	*CLIP1*, *DCLK1*, *FES*, *KIF20B*, *NUSAP1*, *PRC1* (includes EG:233406)
Organization of microtubules	35	5	14	*CDC25B*, *CENPF*, *DST*, *FES*, *PRC1* (includes EG:233406)
Quantity of microtubules	19	5	26	*KIF2C*, *MBP*, *NEK2*, ***STMN1***, *TACC3*
Density of microtubules	7	4	57	*BIRC5*, *KIF2C*, *MBP*, ***STMN1***
Depolymerization of microtubules	37	4	11	*CKAP2*, *KIF18A*, *KIF2C*, ***STMN1***
Destabilization of microtubules	13	3	23	*KIF2C*, ***STMN1***, *TACC3*
Nucleation of microtubules	19	3	16	*BIRC5*, *HAUS8*, *TUBG1*
Growth of microtubules	15	2	13	*BIRC5*, *KIF4A*

*Total number of genes defining gene ontology (GO) function.
†Genes differentially expressed in patient and control ONS cells (P<0.01, false discovery rate corrected, at least twofold difference between patient and control).
Note that *STMN1* (shown in bold), coding for stathmin, a microtubule-severing protein, is common to most of the microtubule-associated functions.

immunoreactivity was significantly less in all regions in patient cells compared with control cells (outer region, t=5.1, d.f.=17, P<0.001; middle region, t=5.31, d.f.=17, P<0.001; inner region, t=3.4, d.f.=17, P<0.01).

The fluorescence intensity of MitoTracker dye (a mitochondrial stain) was quantified within the three defined intracellular regions using automated image analysis. Two-way ANOVA was performed with disease status and region as main effects. Mitochondrial fluorescence in patient cells was significantly different from that in control cells (disease status, $F_{1,51}$=5.92, P<0.05) with significant differences in distributions among the regions (region, $F_{1,51}$=98.02, P<0.0001). Post-hoc Bonferroni adjusted t-tests showed that MitoTracker fluorescence intensity was significantly less in the outer region in patient cells compared with control cells (t=4.1, d.f.=17, P<0.01).

Peroxisomes were identified as spots of PEX14 immunoreactivity and counted within the three defined intracellular regions using automated image analysis. Peroxisome density was quantified as the ratio of the number of peroxisomes divided by the area of each region. Two-way ANOVA was performed with disease status and region as main effects. Peroxisome density in patient cells was significantly different from that in control cells (disease status, $F_{1,51}$=8.48, P<0.01) with a significant interaction between disease and region (disease status*region, $F_{2,51}$=3.96, P<0.05). Post-hoc Bonferroni adjusted t-tests showed that PEX14 immunoreactivity was significantly less in the outer region in patient cells compared with control cells (t=2.7, d.f.=17, P<0.05).

Dynamics of peroxisome movement

Peroxisome movement was quantified for at least 150-250 peroxisomes in ten randomly selected cells for each ONS cell line from controls (n=7 cell lines; 13,871 peroxisomes) and patients (n=6 cell lines; 10,529 peroxisomes). The majority of peroxisomes moved with essentially Brownian motion in random walks back and forth in the same small area. The range of peroxisome speeds was similar in control and patient cells but the distribution of peroxisomes in each speed class were shifted to the left in patient cells compared with control cells, indicating that patient cell peroxisomes were slower, on average (Fig. 5; Chi-square=100.78, d.f.=13, P<0.0001). The mean peroxisome speed in patient cells was 93% slower than in control cells (control, 0.172±0.001 μm/second; patient, 0.160±0.001 μm/second; t=9.19, d.f.= 24,398, P<0.0001). The tracks lengths of some peroxisomes were quite long (control maximum, 77 μm; patient maximum, 49 μm) with the mean track length in patient cells being 95% less than in control cells (control, 10.04±5.90 μm; patient, 9.51±0.5.4 μm; t=7.26, d.f.= 24,398, P<0.0001). Because peroxisome movement was not linear, their distances of displacement from the starting point were shorter than their track lengths (control maximum, 56 μm; patient maximum, 37 μm) with the mean displacement in patient cells being 93% less than in control cells (control, 1.71±0.02 μm; patient, 1.59±0.02 μm; t=4.076, d.f.= 24398, P<0.0001).

Patient cells were smaller than control cells

Cell size was measured by automated image analysis using two methods to visualize the cells: a fluorescent cytoplasmic dye (CellMask) and acetylated α-tubulin immunoreactivity. Both methods demonstrated that patient cell size was 90% of control cell size, with the cytoplasmic dye measuring a larger cell size (CellMask control, 3117 μm^2 ± 154; CellMask patient, 2775 μm^2 ± 114; acetylated α-tubulin control, 2402 μm^2 ± 97; acetylated α-tubulin patient, 2185 μm^2 ± 80). Two-way ANOVA was performed with disease status and labeling method as main effects. Cell size was significantly different in patient and control cells (disease status, $F_{1,140}$=5.90, P<0.05) and there was a significant difference between the labeling methods (labeling method, $F_{1,140}$=32.23, P<0.001). Post-hoc t-tests indicated that control cells were significantly larger than patient cells for the cytoplasmic dye (t=1.78, P<0.05) and for acetylated α-tubulin (t=1.72, P<0.05).

Patient cells and control cells were differentially sensitive to tubulin binding drugs

Cells were exposed to paclitaxel and vinblastine at doses of 0-10 nM. The effects of low doses of these drugs are apparent on visual inspection (supplementary material Figs S5, S6). Both drugs caused acetylated α-tubulin content to increase and caused the cells to

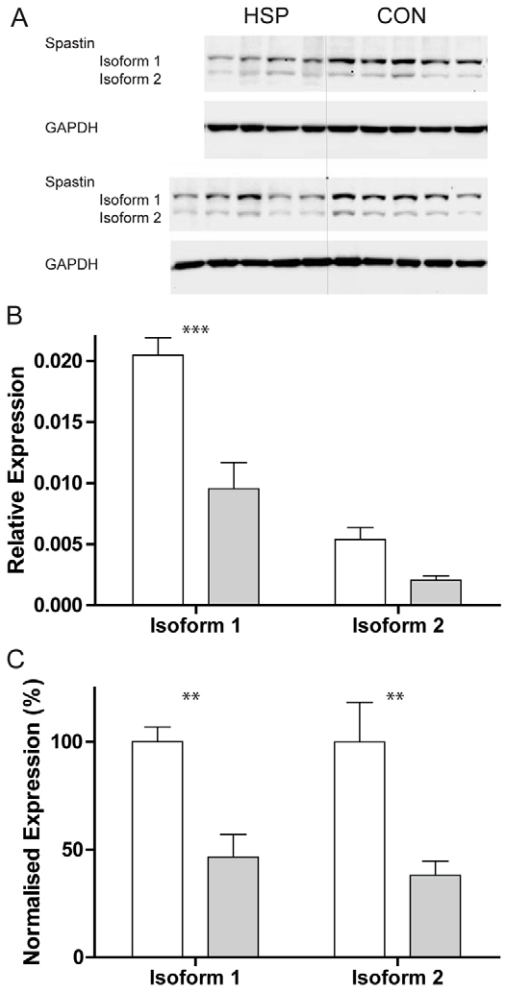

Fig. 2. Patient cells expressed less spastin than controls. (A) Immunoblots showing spastin protein expression in nine patient cell lines (HSP, five left columns) and ten control cell lines (CON, five right columns) and associated loading controls (GAPDH). (B) The expression of each of the spastin isoforms was normalized against the GAPDH loading control and averaged for each group: patient (shaded bars) and control (open bars). (C) The data in B were normalized against the mean expression level of the control group for each isoform and are shown as mean ± s.e.m. Patient and control spastin expression was significantly different. Pair-wise comparisons were using *t*-tests; ***P*<0.001, ****P*<0.001.

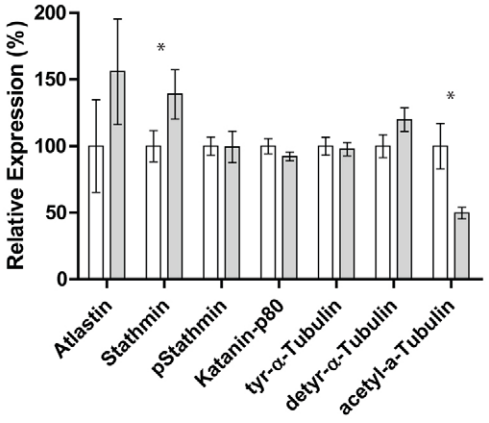

Fig. 3. Microtubule-associated protein expression. Histograms indicate the expression of each of the proteins indicated, normalized against the GAPDH loading control, averaged for each group and normalized against the mean expression level of the control group for each protein: patient (shaded bars) and control (open bars). Values are means ± s.e.m. Pair-wise comparisons were using *t*-tests; **P*<0.05. The immunoblots upon which the figure is based are shown in supplementary material Figs S2-S4.

shrink. These changes were quantified using automated image analysis of acetylated α-tubulin immunoreactivity intensity. Three-way ANOVA was undertaken with disease status, drug, and dose as main effects. There was no significant effect of disease status. There was a significant different differences between drugs ($F_{1,552}$=223.54, P<0.0001) and doses ($F_{5,552}$=635.04, P<0.0001) and a significant interaction between disease status and dose ($F_{5,552}$=6.05, P<0.0001), indicating that patient and control cells responded differently to the drugs in a dose-dependent manner. There was a significant interaction between drug and dose ($F_{5,552}$=75.94, P<0.0001), indicating that paclitaxel and vinblastine had different dose-response profiles. When the data for each drug at 0 nM were combined, control cells had a significantly higher level of acetylated α-tubulin immunofluorescence intensity than patient cells (control cells, 89.8±1.26, n=72; patient cells, 77.8±0.62, n=80; t=9.03, d.f.=142, P<0.0001; Fig. 6A). This repeats and confirms the robust differences in acetylated α-tubulin protein expression already noted. Increasing doses of both drugs eliminated the patient-control difference in acetylated α-tubulin immunofluorescence intensity (Fig. 6B). The main difference between drugs was the level reached, with vinblastine maximal at 5 nM and ~50% of the paclitaxel level, which did not reach maximal at 10 nM.

Cell area was quantified in the same cells by defining the cytoplasm from the spatial extent of acetylated α-tubulin immunoreactivity. At baseline (0 nM drug doses), patient cells were 86% the size of control cells (control cells, 2613±88 μm^2; patient cells, 2260±69 μm^2; t=3.15, d.f.=142, P<0.005; Fig. 6C). This confirms similar relative size of patient cells estimated in two independent experiments noted above (CellMask, 89%; acetylated α-tubulin immunoreactivity, 90%). Both drugs caused all cells to decrease in size (Fig. 6D), but the patient cells remained smaller at all doses of both drugs. Three-way ANOVA was undertaken with disease status, drug, and dose as main effects: disease status and dose were significant (disease status, $F_{1,552}$=36.59, P<0.0001; dose, $F_{5,552}$=24.04, P<0.0001). There was a significant interaction between drug and dose ($F_{5,552}$=4.61, P<0.0001), indicating that paclitaxel and vinblastine had different dose-response profiles.

DISCUSSION

We show here that loss of spastin in patient-derived ONS cells had no effect on cell proliferation or on eight other 'metabolic' functions, although there were significant changes in microtubules and microtubule-associated functions (Table 3). These normal cell functions are in stark contrast to the massive changes in gene expression, affecting 57% of the transcriptome, which clearly demonstrates that patient cells, although appearing

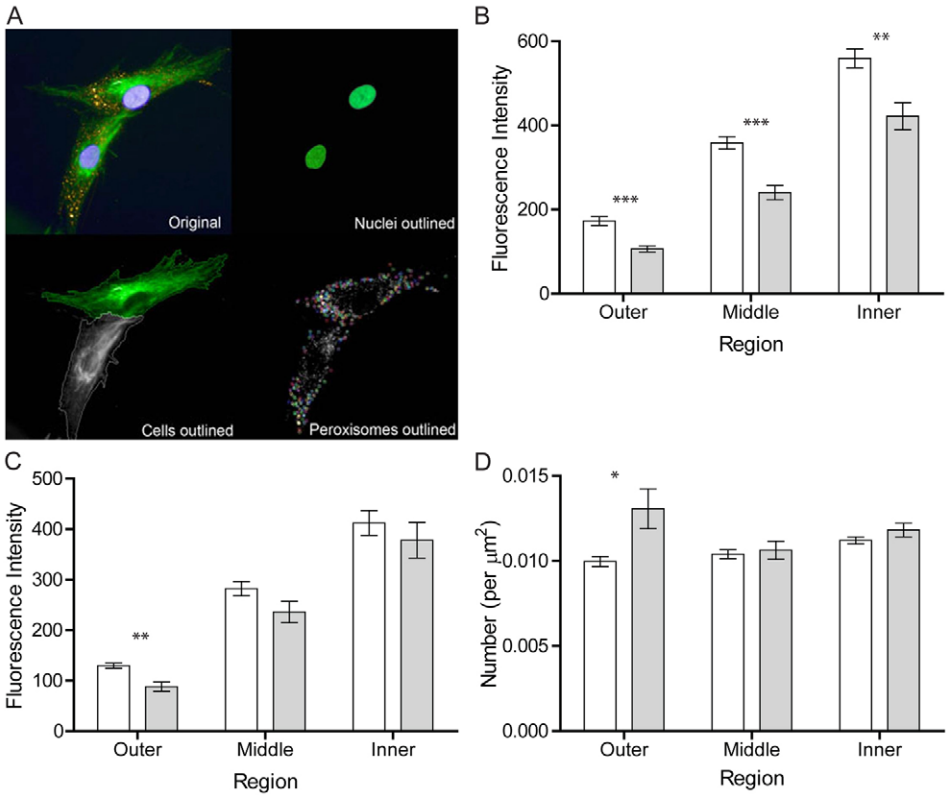

Fig. 4. Altered intracellular distributions of acetylated α-tubulin, mitochondria and peroxisomes. (A) Images of cells showing automated image analysis. Top left panel: Original image of two cells with nuclei (blue, DAPI), acetylated α-tubulin (green, immunofluorescence) and peroxisomes (yellow, PEX14-immunofluoresence). Top right: nuclei (green) identified. Bottom left: Cell boundaries identified; the non-green cell was rejected because it overlaps the edge. Bottom right: Peroxisomes (circles) identified. (B) Acetylated α-tubulin immunofluorescence (stable microtubules) within cellular subregions (outer, middle and inner). Patient cells (shaded bars) expressed significantly less acetylated α-tubulin overall than controls (open bars) (P<0.0001) and less in each region. Examples of images of acetylated α-tubulin immunofluorescence are shown in supplementary material Figs S5, S6. (C) MitoTracker fluorescence (mitochondria) within cytoplasm subregions (outer, middle and inner). Patient cells (shaded bars) had significantly less fluorescence overall than controls (open bars) (P<0.05) with the outer region more greatly affected. (D) PEX14 immunofluorescent peroxisomes within cytoplasm subregions (outer, middle and inner). Patient cells (shaded bars) had significantly more peroxisomes overall than controls (open bars) (P<0.05) with the outer region more greatly affected. Data indicate mean ± s.e.m. Post-hoc Bonferroni pair-wise comparisons: *P<0.05, **P<0.01, ***P<0.001.

'normal', are in an extreme state of regulatory compensation for the loss of spastin. Among the dysregulated genes in patient cells are microtubule-severing genes, tubulin genes and kinesin family genes, associated with tubulin functions in intracellular transport, as well as many other genes associated with microtubule dynamics. We hypothesize that these remarkable changes in gene expression are part of the homeostatic compensation for the 50% reduction of spastin, a microtubule-destabilizing protein, which led to a paradoxical 50% reduction in acetylated α-tubulin, an indicator of stabilized microtubules. The loss of stabilized microtubules can be explained by the 150% increase in expression of stathmin, a microtubule destabilizing protein (Cassimeris, 2002). Further evidence for a failure of homeostasis in patient cells is their smaller size, the altered intracellular distributions of peroxisomes and mitochondria and the slower speeds of peroxisome trafficking (Table 3).

Haploinsufficiency of *SPAST* in patient cells

In patient-derived lymphoblastoid cells with nonsense or frameshift mutations in *SPAST*, neither truncated spastin nor mutated transcripts could be detected, indicating that these mutations lead to loss of spastin function (Charvin et al., 2003). In the present study, this type of *SPAST* mutation had no effect on the amount of spastin protein expressed: average patient cell spastin levels were 50% of control cell levels and levels in all individual patient cells were below control levels. *SPAST* mRNA produces two isoforms of spastin protein, the smaller of which is present in the nucleus and the larger more abundant in the cytoplasm. The larger isoform is also more abundant in brain and spinal cord (Claudiani et al., 2005), specifically in neurons (Charvin et al., 2003). Spastin regulates microtubule dynamics, especially in axons and growth cones (Errico et al., 2002; Park et al., 2010) and it has been argued that the larger isoform might play the major role in the pathogenesis of HSP (Claudiani et al., 2005). Our results show that, like neurons, ONS cells have more of the larger isoform than the smaller isoform and both are reduced to 50% in patient cells with mutations in *SPAST*. The reduced spastin expression in patient cells agrees with inferences from genetic analyses, which indicate that haploinsufficiency is the basis for pathogenesis of HSP in *SPAST* patients (Riano et al., 2009; Solowska et al., 2010).

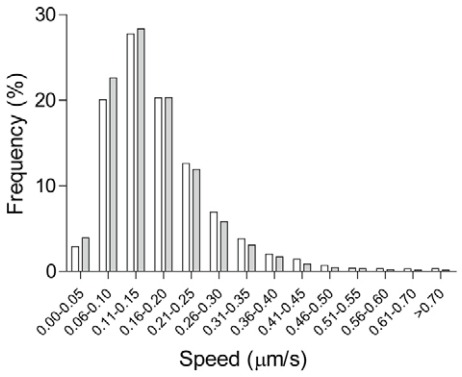

Fig. 5. Peroxisome speeds were slower in patient and control cells. Frequency distributions of peroxisomes in different speed classes are shown for control cells (open bars; *n*=7 individuals, 10 cells per individual) and patient cells (filled bars; *n*=6 individuals, 10 cells per individual). Peroxisome speeds were quantified every 2 seconds for 2 minutes and grouped in speed classes expressed as the percentage of peroxisomes in each speed class as a percentage of the total number of peroxisomes for each group (control cells, *n*=13,871 peroxisomes; patient cells, 10,529 peroxisomes).

Gene expression and *SPAST* mutations

In patient cells, 5723 genes (57% of the total expressed) were differentially expressed compared with control cells ($P<0.01$, corrected for multiple testing). Of these, 1229 were expressed twofold differently. A similar level of dysregulated gene expression was noted in muscle biopsies from three *SPAST* patients in which 2583 genes were differentially expressed ($P<0.05$, twofold difference) (Molon et al., 2004). Inspection of muscle histology demonstrated that it was normal despite the large dysregulation of gene expression (Molon et al., 2004). Taken together, these observations demonstrate that patient tissues and cells can compensate for the massive gene expression dysregulation that follows from spastin insufficiency.

This level of gene expression dysregulation can be considered a 'disease-phenotype' because other patient-control comparisons of ONS cells showed considerably smaller differences in gene expression. In sporadic Parkinson's disease only 500 genes were differentially expressed and in schizophrenia 1700 genes were differentially expressed (Matigian et al., 2010). Those differences in gene expression were associated with altered metabolic functions and oxidative stress in ONS cells from Parkinson's disease patients (Cook et al., 2011; Matigian et al., 2010) and faster proliferation and shorter cell cycle in ONS cells from schizophrenia patients (Fan et al., 2012; Matigian et al., 2010). By contrast, HSP patient-derived ONS cells, with 57% of genes affected, were no different from control cells on the same functional assays that distinguished Parkinson's disease and schizophrenia.

Massively dysregulated gene expression, together with normal cell functions, indicates homeostatic re-regulation of tubulin dynamics because of the reduction in spastin. This was demonstrated by the multiple microtubule-associated functions identified by gene ontology analysis of the differentially expressed genes (Table 2). Tubulin genes were affected (*TUBA1A, TUBA1B, TUBA1C, TUBB2B, TUB2C, TUBB2B, TUBB2C, TUBB4Q, TUBB6, TUBG1, TUBG2*) as well as genes involved in microtubule stability (*STMN1*, *KATNA1*, *KATNB1*, *KATNAL1*, *KATNAL2*, *SPG3A*). Of the latter, as noted above, stathmin (*STMN1*) is a microtubule-depolymerizing enzyme (Cassimeris, 2002; Manna et al., 2006). Katanins (*KATNA1*, *KATNB1*, *KATNAL1*, *KATNAL2*) are members (with spastin) of the AAA-family of microtubule-severing enzymes (Roll-Mecak and McNally, 2010; Yu et al., 2008). Atlastin (*SPG3A*) is a binding partner of spastin whose mutations lead to an autosomal dominant form of HSP similar to that found with *SPAST* mutations, although with childhood onset (Park et al., 2010; Sanderson et al., 2006). Of interest too are many members of the kinesin family of genes whose expression was altered in patient cells (*KIF1B*, *KIF1C, KIF2A, KIF2C, KIF4A, KIF7, KIF11, KIF13B, KIF14, KIF15, KIF18A, KIF20A, KIF20B, KIF23, KIFC1,*

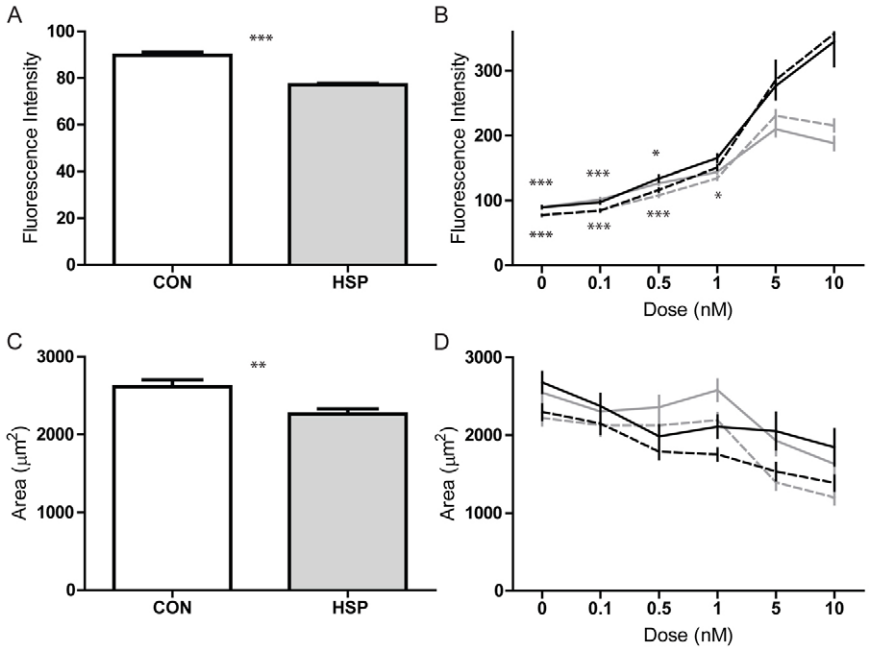

Fig. 6. Effects of paclitaxel and vinblastine. (A) Average intensity of acetylated α-tubulin immunofluorescence in control cells (open bar) and patient cells (shaded bar) at baseline. Control cells expressed significantly more acetylated α-tubulin than patient cells. (B) Effects of paclitaxel (black lines) and vinblastine (grey lines) at 0-10 nM on acetylated α-tubulin immunofluorescence in control cells (continuous lines) and HSP patient cells (dashed lines). Both drugs significantly increased acetylated α-tubulin immunofluorescence, but paclitaxel more so ($P<0.0001$). Control cells were significantly larger than patient cells at 0-0.5 nM paclitaxel (upper asterisks) and at 0-1 nM vinblastine (lower asterisks). (C) Average cell area calculated from acetylated α-tubulin immunofluorescence in control cells (open bar) and patient cells (shaded bar) at baseline. Control cells were significantly larger than patient cells. (D) Effects of paclitaxel (black lines) and vinblastine (grey lines) at 0-10 nM on cell area in control cells (continuous lines) and HSP patient cells (dashed lines). Both drugs reduced cell area in patient and control cells. Data indicate mean ± s.e.m. *$P<0.05$, **$P<0.01$, ***$P<0.001$.

Table 3. Summary of differences between patient and control cells

Patient cell property	Compared with control
Immunophenotype	Similar
Proliferation rate	Similar
Metabolic functions	
Reduced glutathione content	Similar
MTS metabolism	Similar
Proteasome activity	Similar
ATP content	Similar
Lactate dehydrogenase activity	Similar
Caspase 3/7 activity	Similar
Gene expression	57% genes dysregulated
Microtubule-associated GO functions	11 significantly altered
Spastin protein	50%
STMN1 (stathmin) mRNA	260%
Stathmin protein	150%
Acetylated α-tubulin protein	50%
Acetylated α-tubulin intracellular fluorescence	90%
Mitochondria distribution	67% near cell membrane
Peroxisome distribution	131% near cell membrane
Peroxisome movement (speed, displacement)	93%
Cell size	90%
Response to tubulin-binding drugs	Similar

KIFC2). Kinesins are motor proteins responsible for moving organelles, including peroxisomes and mitochondria, along microtubules towards the cell periphery (Daire and Poüs, 2011; Hirokawa and Noda, 2008) and *KIF5A* mutations lead to adult-onset HSP (Blackstone et al., 2011).

Tubulin dynamics and *SPAST* mutations

As a window into microtubule dynamics, we quantified levels of post-translational modifications to α-tubulin: stabilized microtubules become acetylated, tyrosination assists turnover and de-tyrosination assists stability (Hubbert et al., 2002; Kreis, 1987; Piperno et al., 1987; Webster et al., 1987). Patient cells had significantly lower levels of acetylated α-tubulin but similar levels of tyrosinated and de-tyrosinated forms (Fig. 3). Automated image analysis confirmed that patient cells had less acetylated α-tubulin than control cells and that the loss was similar spatially throughout the cells (Fig. 4). The paradoxical loss of acetylated α-tubulin demonstrates the value of investigating the effects of natural *SPAST* mutations in human patient-derived cells. In *Drosophila*, when the homolog of *SPAST*, *Dspastin*, was reduced or mutated genetically, neuronal acetylated α-tubulin was increased (Orso et al., 2005) and overexpression of *Dspastin* decreased acetylated α-tubulin (Trotta et al., 2004). Presumably this paradox is due to species differences in spastin function and regulatory pathways, although cell-type specificity might contribute.

Mitochondria and peroxisomes are organelles whose distribution is dependent on microtubule-assisted transport. They are implicated in the cellular pathology of HSP because long axons (such as those of the corticospinal motor neurons) might be susceptible if microtubule dynamics are dysregulated (Errico et al., 2002; Park et al., 2010). In patient cells, there were fewer mitochondria throughout the cell, with the biggest reduction in the outer region, and there were more peroxisomes in the outer region close to the cell membrane (Fig. 4). The speed of peroxisome movement was slower in patient cells (Fig. 5), leading to significantly shorter track distances and shorter displacement distances. Although the measured peroxisome trafficking deficits in patient cells are small, they represent 93-95% of the values in control cells over the 2-minute observation period. We hypothesize that the differences in the microtubule network and organelle distributions would be amplified in the very long axons of corticospinal motor neurons. Additionally, tubulin dynamics are not the same in the cell body as in long axons (Brown et al., 1992; Conde and Cáceres, 2009); hence, it is of interest to investigate these functions after ONS cells are differentiated into neurons.

We confirmed that stathmin protein, like its mRNA, was overexpressed in patient cells. Stathmin activity is blocked by phosphorylation (Manna et al., 2009), but phosphorylated stathmin protein expression was unaffected in patient cells. The higher levels of activated stathmin could induce greater microtubule destabilization in patient cells (Manna et al., 2006; Manna et al., 2009), leading to the reduced levels of acetylated α-tubulin. Although the mechanism of action is not exactly the same, spastin and stathmin both regulate microtubule dynamics (Manna et al., 2006; Riano et al., 2009) in cooperation with other proteins such as tubulins and kinesins whose genes were differentially expressed in patient cells (Daire and Poüs, 2011; Kreis, 1987). The higher levels of activated stathmin could induce greater microtubule destabilization in patient cells (Manna et al., 2006; Manna et al., 2009). It is plausible therefore that the observed increased levels of stathmin are a result of (over-) compensation for decreased spastin in patient cells.

Increased stathmin expression links HSP to other motor neuron diseases

Type 1 spinal muscular atrophy (SMA) arises from mutations in the gene *SMA*, which leads to muscle weakness because of axon degeneration of the motor nerves (Wen et al., 2010). In type I SMA-like mice, there is a 26% loss of microtubules and a 27% reduction in acetylated α-tubulin in peripheral nerves (Wen et al., 2010). Associated with the loss of stabilized microtubules, stathmin levels are increased in the spinal cords and sciatic nerves, with the protein level correlated with SMA disease severity. Downregulation of stathmin rescues the microtubule network defect and recovers mitochondrial density in sciatic nerves in the SMA-like mouse (Wen et al., 2010). In a model of familial amyotrophic lateral sclerosis, mutant superoxide dismutase (*SOD1*^{G93A}) is associated with a loss of phosphorylated stathmin in the motor neurons in the spinal cord (Strey et al., 2004). Stathmin is active in its unphosphorylated form (Manna et al., 2009) so that loss of phosphorylation indicates increased activity. Concomitantly, in 30% of spinal motor neurons with fragmented Golgi, there is an increase in stathmin in mutant SOD1^{G93A} mice, and stathmin overexpression in HeLa cells led to fragmented Golgi and disrupted microtubule networks (Strey et al., 2004).

The present observations add a further monogenic motor neuron disease that is associated with raised levels of stathmin, reduced actetylated α-tubulin and altered microtubule network. It is notable

that in all these diseases, increased stathmin is a gain-of-function brought about by different genetic mutations, demonstrating that increased stathmin could be a final common pathway to disease pathogenesis, with other factors defining which motor neuron type is affected. When *STMN1* is overexpressed in Purkinje cells of the mouse cerebellum there is disruption of the microtubule network, altered motor protein distribution and loss of function (Ohkawa et al., 2007). It is probable that stathmin levels and activity are regulated according to the demands of each specific cell type and this could explain the specificity of clinical manifestations in different motor neuron diseases. Large, heavily myelinated motor neurons might be specifically sensitive to dysregulated stathmin functions but are able to compensate until cellular mechanisms associated with cell type and age interact to lead to disease onset.

Differential sensitivity to microtubule-binding drugs in patient cells

At the low doses used here (0-1 nM), both paclitaxel and vinblastine increased the levels of acetylated α-tubulin in ONS cells but paclitaxel had a larger effect than vinblastine. Paclitaxel binds to stabilized microtubules (Giannakakou et al., 1998) and pulls the equilibrium of microtubule formation towards the stable state, as measured by acetylated α-tubulin. Vinblastine binds to tubulin dimers (Giannakakou et al., 1998) and will bias the equilibrium towards that state. Our results indicate that low doses of paclitaxel or vinblastine (less than 0.1-0.5 nM) restored the levels of acetylated α-tubulin in patient cells to the levels found in control cells at baseline (0 nM). Vinblastine ameliorated the behavioral and cytological deficits associated with the *SPAST/Dspastin* mutations in *Drosophila* (Orso et al., 2005), but in that model acetylated α-tubulin expression was increased compared with controls, not reduced as seen in patient ONS cells. Noscapine, another microtubule-binding drug, delayed the onset of disease in type I SMA-like mice, which have increased stathmin levels in their affected motor neurons (Wen et al., 2010). Our results suggest that low-dose microtubule-binding drugs are potential leads for therapy in HSP and perhaps other motor neuron diseases with raised stathmin levels.

Patient-derived olfactory stem cells as models for HSP

These investigations present a new understanding of the cellular consequences of mutations in *SPAST* in patient cells. They indicate that the primary disease mechanism is haploinsufficiency of *SPAST* and the consequent reduced expression of spastin, but suggest a new hypothesis, i.e. that homeostatic compensation for loss of spastin leads to overexpression of stathmin, which subsequently disrupts microtubules and organelle distribution. *SPAST* mutations in patient-derived ONS cells leave many cell functions intact but do affect cell functions such as tubulin stability and organelle transport, which might be amplified in the long axons of corticospinal motor neurons. Patient-derived ONS cells offer advantages over transgenic animal and other cell models because the effect of natural *SPAST* mutations are seen against the normal human genetic background that contributes to the variation of penetrance and severity of HSP in patients with the same mutated gene.

An advantage of ONS cells is that they can be grown in standardized conditions in the quantities needed for in-vitro drug screening, demonstrated in the differential responses of ONS cells to the tubulin-binding drugs paclitaxel and vinblastine. ONS cells can be differentiated into neurons (Murrell et al., 2005), which might show additional disease-specific deficits because axons are more dependent than the cell body on microtubule-based transport. Although applied here to patients with mutations in *SPAST*, the model is also applicable to patients with other genetic forms in the hereditary spastic paraplegia family.

MATERIALS AND METHODS

Participants and nasal biopsies

HSP patients were reviewed and examined by a neurologist (C.M.S.). Specific questioning to confirm the age of onset, disease duration, family history, use of walking aids and sphincter dysfunction was performed. Patients (n=9) were examined for signs of upper and lower limb spasticity and weakness, hyper-reflexia, ataxia, sensory abnormalities, gait abnormalities and saccadic abnormalities. All had very similar clinical features, typical of adult onset hereditary spastic paraplegia. They were subsequently identified as having mutations in *SPAST* (Table 1). Controls (n=10) were recruited from the general population. Olfactory mucosa biopsies were taken as described (Féron et al., 1998) and obtained with the written, informed consent of the subjects. All procedures were carried out in accordance with the human ethics committee of Griffith University and the Northern Sydney and Central Coast Human Research Ethics Committee, and according to guidelines of the National Health and Medical Research Council of Australia. Participant details are briefly summarized in Table 1, including sex, age and identified *SPAST* mutations, which are fully described elsewhere (Vandebona et al., 2012).

Cell culture

From each biopsy, olfactory neural progenitor cultures were prepared, stored frozen and thawed for analysis as described (Matigian et al., 2010; Murrell et al., 2005). This involved dissociating the olfactory tissues, culturing them for 3 days as primary cultures in serum-containing medium and growing them in serum-free medium containing epidermal growth factor (EGF) and basic fibroblast growth factor (FGF2) to generate neurospheres. Free-floating neurospheres were dissociated and grown as adherent cultures in serum-containing medium, after which they were frozen and stored in liquid nitrogen. We refer to these cultures as olfactory neurosphere-derived (ONS) cells (Matigian et al., 2010). Frozen aliquots of ONS cells were used as the starting point for all the experiments described. All cultures were grown to 80% confluency under standard conditions on tissue culture plastic in DMEM/F12 (Gibco) supplemented with 10% fetal bovine serum (FBS) at 37°C and 5% CO_2.

Cell function assays

Cell function assays were performed as described previously (Matigian et al., 2010). Briefly, ONS cells were grown in DMEM/F12 supplemented with 10% FBS, harvested using TrypLE Express (Invitrogen), washed in HBSS and resuspended in 10 ml of growth medium. Cell counts were performed using an automated particle counter (Beckman Coulter); cells were diluted to 2.5×10^4 cells/ml and 2500 cells (100 µl) were seeded into triplicate wells of 96-well plates [clear (absorbance based), white

(luminescence-based) or black (fluorescence-based) as appropriate (Nunc)] and allowed to attach overnight. Medium was changed 24 hours prior to assay. All plates and reagents were equilibrated to room temperature prior to assay initiation and all results were obtained using a Synergy II plate reader (BioTek). Reduced glutathione (GSH) content was determined using modified manufacturer-supplied protocols (GSH-Glo Glutathione Assay, Promega). Medium was aspirated and cells washed twice in HBSS (100 µl per well), then 50 µl of reaction buffer was added to each well and plates were incubated at room temperature for 15 minutes, with light protection. Luciferin detection reagent (50 µl) was added and after a further 15 minutes of light-protected incubation, luminescence intensity was recorded. MTS assay (CellTiter aqueous MTS assay protocol, Promega), chymotrypsin-like proteasome activities (Cell-Based Proteasome-Glo Assays, Promega), ATP levels (ATPlite assay kit, Perkin Elmer), lactate dehydrogenase activity (CytoTox-ONE Homogenous Membrane Integrity Assay, Promega) and caspase-3 and caspase-7 activities (Apo-ONE Homogenous Caspase-3/7 Assay, Promega) were measured according to manufacturer-supplied protocols. Data were normalized to DNA content, determined using supplied protocols (CyQUANT-NF, Invitrogen; 50 µl of prepared reagent per well, including medium-only control wells). For each cell line, triplicate values from each assay were averaged and a signal:DNA content ratio determined.

Cell proliferation

Each patient and control cell line was seeded at 2500 cells/cm^2 in 96-well plates. At 24, 48 and 72 hours, relative cell numbers were assessed. At each time point, DNA content was quantified in three wells from each patient and control ONS cell line using CyQUANT-NF as described above. For analysis, the DNA content of each ONS cell line at each time point was normalized against its own average DNA content at 24 hours, to control for small differences in starting populations. Statistical analysis was conducted using a two-tailed unpaired *t*-test (GraphPad Prism 5 for Windows).

Flow cytometry

ONS cells were fixed in paraformaldehyde (4% in HBSS) for 10 minutes at room temperature. Approximately 1×10^5 cells were washed twice with HBSS and incubated for 30 minutes at room temperature in 0.2 ml permeabilization buffer (HBSS containing 1% BSA, 1% normal goat serum and 0.1% Triton X-100) together with primary antibody. Following incubation, cells were washed twice in HBSS containing 1% BSA and incubated for 30 minutes at room temperature with 1:800 dilution of the appropriate fluorescently labeled secondary antibody. After two washes, the cells were resuspended in washing buffer. The fluorescence intensity of samples was then analyzed by flow cytometry (BD FACSAria flow cytometer, equipped with a Coherent Sapphire Solid State 488 laser and JDS Uniphase HeNe Air Cooled 633 laser). For all antibody-staining experiments, isotype matched controls were run in parallel. Positive staining was assessed as the fluorescence intensity greater than that associated with the isotype-matched controls. Analysis was performed using FloJo version 7.2.5 (Tree Star, Ashland, OR). Data are presented as mean ± s.e.m. of cells expressing each marker averaged across nine patient cell lines and ten control cell lines.

Gene expression profiling

Two separate aliquots ('biological replicates') of ONS cells from the 19 participants were grown and profiled using the Illumina Beadarray arrays, producing 38 gene expression profiles, as described (Matigian et al., 2010). Additional 'biopsy replicates' were provided by ONS cells generated from three control patients who were biopsied twice in different regions of the olfactory mucosa. For mRNA extraction, ONS cells were grown until 80-90% confluent to assure similar growth phase and optimized mRNA yield. Total RNA was isolated using QIAGEN RNeasy Mini Kit using an on-column DNase I treatment. All RNA preparations were quantified using a Nanodrop ND1000 and checked with an Agilent 2100 Bioanalyzer (RNA nanochips): only samples with RNA integrity number (RIN) >9 were accepted for RNA amplification. Each RNA sample was labeled using the Ambion Illumina RNA Amplification Kit and hybridized to human whole-genome Illumina Human-Refseq8v3 BeadChips (Illumina, San Diego, CA). The raw data from BeadStudio was background-adjusted and quantile-normalized using the lumi package in R/BioConductor (Du et al., 2008). The normalized data were exported from R/BioConductor for further analysis in Genespring GX 7.3.1. software (Agilent Technologies, Mulgrave, Australia).

Comparison of the raw fluorescence intensities on the arrays from duplicate biopsies (i.e. ONS cells generated from separate biopsies) from each participant provided an estimate of the experimental variability arising from the culture procedure, RNA preparation and gene expression profiling. Comparison of the raw fluorescence intensities on the arrays from biopsy replicate samples from three control participants provided an estimate of the experimental variability arising from the region of biopsy, the primary culturing procedure and the freezing protocol as well as the variables between the biological replicates. The correlation in raw fluorescence between the biological replicates was very high (r^2=0.98, n=20). The correlation in raw fluorescence between the duplicate biopsies was also very high (r^2=0.96, n=3). The correlation in raw fluorescence between individual participants was less, but still high within the groups (control, r^2=0.94, n=10; HSP, r^2=0.93, n=10). Because intra-individual variability was less than inter-individual variability, subsequent analyses were performed on the average of raw fluorescence values for each gene (probe) across all replicates. Genes were initially filtered using Illumina detection score. A gene (probe) was included in further analysis if it had a detection score ≥0.99 in both biological replicate samples and in more than 50% of individuals within the patient or the control group. This procedure generated a list of genes expressed in the cells.

Gene ontology analysis

To determine genes that were differentially expressed in disease and control samples, the gene list was subjected to a parametric ANOVA ($P\leq0.01$) and P values adjusted for multiple testing using the Benjamini and Hochberg false discovery rate method; a fold change cut-off greater than ±2 was applied for some analyses. The advantage of this analysis was the identification of genes whose expression was not altered with biological replicate, providing a list of genes that were differentially expressed in disease states compared with controls. The lists of differentially expressed genes for each disease were then subjected to pathway 'over-

representation' analysis using Ingenuity Pathway Analysis (IPA) 6.0 (Ingenuity Systems, Redwood City, CA). Over-representation is a measure of the probability that a gene list contains more members of a biochemical pathway than would be expected by chance, given the number of theoretical members in a pathway, the number of members in the list of genes of interest and the number of genes used to generate the list of interest (i.e. the probes on the Illumina Ref8v3 BeadChip). This probability is determined by a right-tailed Fisher's exact test. The criterion for significance was α=0.01.

qRT-PCR confirmation of gene expression

Quantitative real-time PCR (qRT-PCR) was performed as described previously. Briefly cDNA was synthesized from 2 μg of total RNA extracted from ONS cells using Superscript VILO cDNA Synthesis Kit (Invitrogen) according to the manufacturer's protocol. All qRT-PCR reactions were carried out using the commercial master mix Sensimix HRM with Evagreen dye (Quantace, London, UK) on a RotorGene 6000 system (Corbett Technologies, Sydney, Australia) using 5 μl of cDNA (1:10 dilution), and 0.5 μM of gene-specific primers to a total reaction volume of 15 μl. Cycling conditions were as follows: 10 minutes at 95°C followed by 40 cycles with denaturation for 15 seconds at 95°C, annealing for 10 seconds at 55-58°C and elongation for 10 seconds at 72°C. For annealing temperature and primer sequence see supplementary material Table S4. Melting curves were generated after each run to confirm a single PCR product. All reactions were performed in triplicate and in each run an internal standard curve was used to assign relative concentrations to the amplicons. All qRT-PCR primers were designed using ExPrimer (Sandhu and Acharya, 2005) and Primer3 (http://frodo.wi.mit.edu/), and were synthesized by Sigma-Aldrich. Sequences and exon information used for primer design were obtained from public databases (GenBank, NCBI and Ensembl). BLAST searches were performed to confirm the total gene specificity of the primer sequences. Fluorescence data were converted into cycle threshold measurements using the RotorGene 6000 series software version 1.7. The data were analyzed using REST 2008 software (http://www.gene-quantification.info/) and compared statistically by pair-wise fixed reallocation randomization test (Pfaffl et al., 2002). Relative expression of target mRNA was normalized against *EEF1A1* mRNA, because it displayed the least variation within the microarray experiments, and quantified using a relative quantification approach with efficiency correction (Pfaffl et al., 2002).

Immunoblot analysis

Cells were cultured on plastic as described above to ~80% confluence and washed three times in phosphate-buffered saline (PBS) and lysed with RIPA (25 mM Tris-HCl pH 7.4, 2 mM EDTA, 150 mM NaCl, 1% Triton X-100, 1 mM NaF, 0.25% sodium deoxycholate, 0.2 mM Na_3VO_4, 1× protease inhibitors cocktail). Protein concentration of cell lysates was determined using a DC protein assay kit (Bio-Rad). Equal total amount of proteins (10 μg) were loaded onto a 10% denaturing sodium dodecyl sulfate-PAGE (SDS-PAGE) gel. After electrophoresis, the gels were electroblotted onto polyvinylidine difluoride membranes, blocked with Tris-buffered saline containing 5% milk and 0.1% Tween 20 for 1 hour and incubated overnight at 4°C with the primary antibody (anti-aceylated α-tubulin, 1:1000, ab24610, Abcam; anti-spastin, 1:250, ab77144, Abcam; anti-katanin P80, 1:1000, ab37555, Abcam; anti-SPG3A, 1:300, ab58273, Abcam; anti-Stathmin, 1:1000, ab52630, Abcam; anti-GAPDH, 1:10,000). Immunoreactivity was visualized with a secondary horseradish peroxidase (HRP)-conjugated anti-rabbit, HRP-conjugated anti-mouse antibody or HRP-conjugated anti-chicken antibody, using the enhanced chemiluminescence system according to the manufacturer's instructions. The quantification of immunoblotting was analyzed using the Quantity One program (Bio-Rad), normalizing against GAPDH immunoreactivity in each sample as an internal control.

High content imaging and automated image analysis

ONS cells were grown in DMEM/F12 supplemented with 10% FBS, harvested using TrypLE Express (Invitrogen), washed in HBSS and resuspended in 10 ml of growth medium. Cell counts were performed using an automated particle counter (Beckman Coulter), and 3000 cells were seeded into triplicate wells of 96-well plates (GE Matriplates). Plates were pre-coated with 1 μg/cm^2 10 μg/ml poly-L-lysine for 4 hours at 37°C. After culturing for 24 hours, the cells were fixed in paraformaldehyde (4% in HBSS) for 5 minutes at room temperature.

Cells were immunostained with antibodies against acetylated α-tubulin (1:1000; ab24610, Abcam) and/or peroxisomes (anti-PEX14, 1:1000) (Nguyen et al., 2006). Cells were washed twice in PBS and incubated for 30 minutes at room temperature with 1:400 dilution of the secondary antibody (goat anti-mouse Alexa Fluor 488, A11001, and goat anti-rabbit Alexa Fluor 594, A11012, Invitrogen). After two washes with PBS, the cells were stained with DAPI (1:1000) for 10 minutes at room temperature. The cells were then washed twice in PBS and 15 images collected per well on an Operetta high content imaging system (Perkin Elmer). For mitochondrial staining, cells were stained with 400 nm Mitotracker Red CMXRos (M7512, Invitrogen) for 30 minutes prior to fixation. The cells were washed twice with PBS and permeabilized for 30 minutes at room temperature in PBS containing 3% BSA and 0.1% Triton-X 100. For the cell size analysis, after fixation by 4% paraformaldehyde for 10 minutes, cells were permeabilized for 30 minutes at room temperature in PBS containing 3% BSA and 0.1% Triton-X 100 and stained in 100 μl of HCS CellMask solution (2 ng/ml; Invitrogen) for 30 minutes at room temperature. Each well was washed two or three times in PBS to remove excess stain before imaging.

The images were analyzed using Harmony High Content Analysis Software (Perkin Elmer). Each cell nucleus was identified using the DAPI stain, after which the cell cytoplasm was defined from CellMask fluorescence or low background acetylated α-tubulin staining (defined as 'cell'). The cytoplasm was then automatically segmented into the three cytoplasmic sub-regions: outer region (adjacent to the cell membrane), middle region (central part of cytoplasm bordering the outer and inner regions) and inner region (adjacent to the nucleus). Parameters of interest (cell size, acetylated α-tubulin fluorescence intensity, peroxisome number and mitochondrial fluorescence intensity) were quantified in each defined cytoplasmic region. For each cell line, 15 images were taken at 400× magnification, from three wells. In the analysis, all cells that overlapped the border of the image were excluded from the analysis.

Dynamics of peroxisome movement

Cells were cultured on 96-well glass plates (Matriplate; MGB096-1-2-LG-L) coated with poly-L-lysine (10 μg/ml). After 24 hours,

the cells were transduced using a CellLight reagent for peroxisome fluorescence (C10604, CellLight Peroxisome-GFP BacMam 2.0) by incubating for 24 hours. The cells were then checked for fluorescence. Peroxisome movement was observed using a Zeiss AxioObserver Z1 microscope. Time-lapse images of fluorescent peroxisomes were acquired under high magnification (63× oil immersion objective; Zeiss AxioObserver Z1 microscope with AxioCamHs camera). Microscope control and image capture were accomplished using Zeiss AxioVision software (AxioVs40 V 4.8.2.0). In each imaging session, peroxisomes within a field of view were acquired in three dimensions every 2 seconds for a total recording time of 2 minutes. Using Imaris software (Imaris×64 6.4.2), individual peroxisomes were identified on the basis of fluorescence intensity and diameter. The peroxisomes were identified using the 'spot' function and a filter was set to track all spots in the field of view for the 2-minute observation period. From the tracks, the following data were collected for each peroxisome: mean speed (micrometers/second), distance traveled (micrometers) and displacement distance (distance between start and finish locations, micrometers).

Effects of microtubule-stabilizing drugs

ONS cells from patients and controls were grown to 70-80% confluence and re-plated in poly-L-lysine pre-coated 96-well plates (3000 cells/well) in duplicate. Then, the cells were treated with paclitaxel and vinblastine at 0, 0.1, 0.5, 1.0, 5.0 or 10 nM for 24 hours. Each concentration was repeated in triplicate in two separate experiments. Cells were then fixed and processed for immunochemistry automated image analysis, as described above. For this analysis, 56 images were taken per well at 200× magnification. In the analysis, any cells that overlapped the border of the image were excluded from the analysis. All images were taken under exactly the same time and exposure. For illustrative purposes only, images were adjusted for brightness using Adobe Photoshop v12.1 (Adobe Systems Incorporated). To obviate observer bias, the image analysis was automated using the same parameters for each image.

Statistical analysis

Data are expressed as mean ± s.e.m. Gene expression analysis is described above. Analyses of variance (ANOVA) of cell function and cell imaging data, and Chi-square analysis of time-lapse data were conducted using SPSS v20 for Windows (IBM SPSS Statistics). Post-hoc, pair-wise comparisons were made with two-tailed *t*-tests adjusted for multiple comparisons with the Bonferroni correction using GraphPad (Prizm). Protein data were analyzed by independent two-tailed *t*-tests. An α-value less than 0.05 was considered statistically significant.

Access to microarray data

Microarray data are available at ArrayExpress (www.ebi.ac.uk/arrayexpress) under accession number E-TABM-724.

ACKNOWLEDGEMENTS

We are very grateful to the individuals who participated in this study and the Hereditary Spastic Paraplegia Research Foundation Incorporated for continuing discussion and support. Thanks to Dr Denis Crane for the PEX14 antibody.

COMPETING INTERESTS

The authors declare that they do not have any competing or financial interests.

AUTHOR CONTRIBUTIONS

G.A., Y.F., S.A.W., C.M.S. and A.M.-S. conceived and designed the experiments. C.M.S. and D.V. undertook patient diagnosis, nasal biopsy and primary cell culture. R.S. established, banked and managed the cell lines and assisted in statistical analysis. G.A., Y.F., N.M., G.W., B.B., R.S. and J.R. performed the experiments. A.M.-S. performed the statistical analyses and wrote the paper. All authors contributed to and edited the paper. A.M-S. and C.M.S. provided funding for the research.

FUNDING

This work was supported by grants from the Australian Government Department of Health and Ageing to establish the National Centre for Adult Stem Cell Research (to A.M.-S.); from the National Health and Medical Research Council [grant number 1028826 to A.M.-S. and C.M.S.]; and the Hereditary Spastic Paraplegia Research Foundation Incorporated (to A.M.-S.).

SUPPLEMENTARY MATERIAL

Supplementary material for this article is available at http://dmm.biologists.org/lookup/suppl/doi:10.1242/dmm.010884/-/DC1

REFERENCES

Blackstone, C., O'Kane, C. J. and Reid, E. (2011). Hereditary spastic paraplegias: membrane traffic and the motor pathway. *Nat. Rev. Neurosci.* **12**, 31-42.

Brown, A., Slaughter, T. and Black, M. M. (1992). Newly assembled microtubules are concentrated in the proximal and distal regions of growing axons. *J. Cell Biol.* **119**, 867-882.

Cassimeris, L. (2002). The oncoprotein 18/stathmin family of microtubule destabilizers. *Curr. Opin. Cell Biol.* **14**, 18-24.

Charvin, D., Cifuentes-Diaz, C., Fonknechten, N., Joshi, V., Hazan, J., Melki, J. and Betuing, S. (2003). Mutations of SPG4 are responsible for a loss of function of spastin, an abundant neuronal protein localized in the nucleus. *Hum. Mol. Genet.* **12**, 71-78.

Claudiani, P., Riano, E., Errico, A., Andolfi, G. and Rugarli, E. I. (2005). Spastin subcellular localization is regulated through usage of different translation start sites and active export from the nucleus. *Exp. Cell Res.* **309**, 358-369.

Conde, C. and Cáceres, A. (2009). Microtubule assembly, organization and dynamics in axons and dendrites. *Nat. Rev. Neurosci.* **10**, 319-332.

Cook, A. L., Vitale, A. M., Ravishankar, S., Matigian, N., Sutherland, G. T., Shan, J., Sutharsan, R., Perry, C., Silburn, P. A., Mellick, G. D. et al. (2011). NRF2 activation restores disease related metabolic deficiencies in olfactory neurosphere-derived cells from patients with sporadic Parkinson's disease. *PLoS ONE* **6**, e21907.

Daire, V. and Poüs, C. (2011). Kinesins and protein kinases: key players in the regulation of microtubule dynamics and organization. *Arch. Biochem. Biophys.* **510**, 83-92.

Deluca, G. C., Ebers, G. C. and Esiri, M. M. (2004). The extent of axonal loss in the long tracts in hereditary spastic paraplegia. *Neuropathol. Appl. Neurobiol.* **30**, 576-584.

Du, P., Kibbe, W. A. and Lin, S. M. (2008). lumi: a pipeline for processing Illumina microarray. *Bioinformatics* **24**, 1547-1548.

Errico, A., Ballabio, A. and Rugarli, E. I. (2002). Spastin, the protein mutated in autosomal dominant hereditary spastic paraplegia, is involved in microtubule dynamics. *Hum. Mol. Genet.* **11**, 153-163.

Fan, Y., Abrahamsen, G., McGrath, J. J. and Mackay-Sim, A. (2012). Altered cell cycle dynamics in schizophrenia. *Biol. Psychiatry* **71**, 129-135.

Féron, F., Perry, C., McGrath, J. J. and Mackay-Sim, A. (1998). New techniques for biopsy and culture of human olfactory epithelial neurons. *Arch. Otolaryngol. Head Neck Surg.* **124**, 861-866.

Giannakakou, P., Villalba, L., Li, H., Poruchynsky, M. and Fojo, T. (1998). Combinations of paclitaxel and vinblastine and their effects on tubulin polymerization and cellular cytotoxicity: characterization of a synergistic schedule. *Int. J. Cancer* **75**, 57-63.

Hedera, P., Eldevik, O. P., Maly, P., Rainier, S. and Fink, J. K. (2005). Spinal cord magnetic resonance imaging in autosomal dominant hereditary spastic paraplegia. *Neuroradiology* **47**, 730-734.

Hirokawa, N. and Noda, Y. (2008). Intracellular transport and kinesin superfamily proteins, KIFs: structure, function, and dynamics. *Physiol. Rev.* **88**, 1089-1118.

Hubbert, C., Guardiola, A., Shao, R., Kawaguchi, Y., Ito, A., Nixon, A., Yoshida, M., Wang, X. F. and Yao, T. P. (2002). HDAC6 is a microtubule-associated deacetylase. *Nature* **417**, 455-458.

Kasher, P. R., De Vos, K. J., Wharton, S. B., Manser, C., Bennett, E. J., Bingley, M., Wood, J. D., Milner, R., McDermott, C. J., Miller, C. C. et al. (2009). Direct evidence for axonal transport defects in a novel mouse model of mutant spastin-induced hereditary spastic paraplegia (HSP) and human HSP patients. *J. Neurochem.* **110**, 34-44.

Kreis, T. E. (1987). Microtubules containing detyrosinated tubulin are less dynamic. *EMBO J.* **6**, 2597-2606.

Mackay-Sim, A. (2012). Concise review: patient-derived olfactory stem cells: new models for brain diseases. *Stem Cells* **30**, 2361-2365.

Manna, T., Thrower, D., Miller, H. P., Curmi, P. and Wilson, L. (2006). Stathmin strongly increases the minus end catastrophe frequency and induces rapid treadmilling of bovine brain microtubules at steady state in vitro. *J. Biol. Chem.* **281**, 2071-2078.

Manna, T., Thrower, D. A., Honnappa, S., Steinmetz, M. O. and Wilson, L. (2009). Regulation of microtubule dynamic instability in vitro by differentially phosphorylated stathmin. *J. Biol. Chem.* **284**, 15640-15649.

Mar, J. C., Matigian, N. A., Mackay-Sim, A., Mellick, G. D., Sue, C. M., Silburn, P. A., McGrath, J. J., Quackenbush, J. and Wells, C. A. (2011). Variance of gene expression identifies altered network constraints in neurological disease. *PLoS Genet.* **7**, e1002207.

Matigian, N., Abrahamsen, G., Sutharsan, R., Cook, A. L., Vitale, A. M., Nouwens, A., Bellette, B., An, J., Anderson, M., Beckhouse, A. G. et al. (2010). Disease-specific, neurosphere-derived cells as models for brain disorders. *Dis. Model. Mech.* **3**, 785-798.

McDermott, C. J., Grierson, A. J., Wood, J. D., Bingley, M., Wharton, S. B., Bushby, K. M. and Shaw, P. J. (2003). Hereditary spastic paraparesis: disrupted intracellular transport associated with spastin mutation. *Ann. Neurol.* **54**, 748-759.

Molon, A., Di Giovanni, S., Chen, Y. W., Clarkson, P. M., Angelini, C., Pegoraro, E. and Hoffman, E. P. (2004). Large-scale disruption of microtubule pathways in morphologically normal human spastin muscle. *Neurology* **62**, 1097-1104.

Murrell, W., Féron, F., Wetzig, A., Cameron, N., Splatt, K., Bellette, B., Bianco, J., Perry, C., Lee, G. and Mackay-Sim, A. (2005). Multipotent stem cells from adult olfactory mucosa. *Dev. Dyn.* **233**, 496-515.

Nguyen, T., Bjorkman, J., Paton, B. C. and Crane, D. I. (2006). Failure of microtubule-mediated peroxisome division and trafficking in disorders with reduced peroxisome abundance. *J. Cell Sci.* **119**, 636-645.

Ohkawa, N., Hashimoto, K., Hino, T., Migishima, R., Yokoyama, M., Kano, M. and Inokuchi, K. (2007). Motor discoordination of transgenic mice overexpressing a microtubule destabilizer, stathmin, specifically in Purkinje cells. *Neurosci. Res.* **59**, 93-100.

Orso, G., Martinuzzi, A., Rossetto, M. G., Sartori, E., Feany, M. and Daga, A. (2005). Disease-related phenotypes in a Drosophila model of hereditary spastic paraplegia are ameliorated by treatment with vinblastine. *J. Clin. Invest.* **115**, 3026-3034.

Park, S. H., Zhu, P. P., Parker, R. L. and Blackstone, C. (2010). Hereditary spastic paraplegia proteins REEP1, spastin, and atlastin-1 coordinate microtubule interactions with the tubular ER network. *J. Clin. Invest.* **120**, 1097-1110.

Pfaffl, M. W., Horgan, G. W. and Dempfle, L. (2002). Relative expression software tool (REST) for group-wise comparison and statistical analysis of relative expression results in real-time PCR. *Nucleic Acids Res.* **30**, e36.

Piperno, G., LeDizet, M. and Chang, X. J. (1987). Microtubules containing acetylated alpha-tubulin in mammalian cells in culture. *J. Cell Biol.* **104**, 289-302.

Riano, E., Martignoni, M., Mancuso, G., Cartelli, D., Crippa, F., Toldo, I., Siciliano, G., Di Bella, D., Taroni, F., Bassi, M. T. et al. (2009). Pleiotropic effects of spastin on neurite growth depending on expression levels. *J. Neurochem.* **108**, 1277-1288.

Roll-Mecak, A. and McNally, F. J. (2010). Microtubule-severing enzymes. *Curr. Opin. Cell Biol.* **22**, 96-103.

Salinas, S., Carazo-Salas, R. E., Proukakis, C., Schiavo, G. and Warner, T. T. (2007). Spastin and microtubules: Functions in health and disease. *J. Neurosci. Res.* **85**, 2778-2782.

Salinas, S., Proukakis, C., Crosby, A. and Warner, T. T. (2008). Hereditary spastic paraplegia: clinical features and pathogenetic mechanisms. *Lancet Neurol.* **7**, 1127-1138.

Sanderson, C. M., Connell, J. W., Edwards, T. L., Bright, N. A., Duley, S., Thompson, A., Luzio, J. P. and Reid, E. (2006). Spastin and atlastin, two proteins mutated in autosomal-dominant hereditary spastic paraplegia, are binding partners. *Hum. Mol. Genet.* **15**, 307-318.

Sandhu, K. S. and Acharya, K. K. (2005). ExPrimer: to design primers from exon-exon junctions. *Bioinformatics* **21**, 2091-2092.

Solowska, J. M., Garbern, J. Y. and Baas, P. W. (2010). Evaluation of loss of function as an explanation for SPG4-based hereditary spastic paraplegia. *Hum. Mol. Genet.* **19**, 2767-2779.

Strey, C. W., Spellman, D., Stieber, A., Gonatas, J. O., Wang, X., Lambris, J. D. and Gonatas, N. K. (2004). Dysregulation of stathmin, a microtubule-destabilizing protein, and up-regulation of Hsp25, Hsp27, and the antioxidant peroxiredoxin 6 in a mouse model of familial amyotrophic lateral sclerosis. *Am. J. Pathol.* **165**, 1701-1718.

Trotta, N., Orso, G., Rossetto, M. G., Daga, A. and Broadie, K. (2004). The hereditary spastic paraplegia gene, spastin, regulates microtubule stability to modulate synaptic structure and function. *Curr. Biol.* **14**, 1135-1147.

Vandebona, H., Kerr, N. P., Liang, C. and Sue, C. M. (2012). SPAST mutations in Australian patients with hereditary spastic paraplegia. *Int. Med. J.* **42**, 1342-1347.

Webster, D. R., Gundersen, G. G., Bulinski, J. C. and Borisy, G. G. (1987). Differential turnover of tyrosinated and detyrosinated microtubules. *Proc. Natl. Acad. Sci. USA* **84**, 9040-9044.

Wen, H. L., Lin, Y. T., Ting, C. H., Lin-Chao, S., Li, H. and Hsieh-Li, H. M. (2010). Stathmin, a microtubule-destabilizing protein, is dysregulated in spinal muscular atrophy. *Hum. Mol. Genet.* **19**, 1766-1778.

Yu, W., Qiang, L., Solowska, J. M., Karabay, A., Korulu, S. and Baas, P. W. (2008). The microtubule-severing proteins spastin and katanin participate differently in the formation of axonal branches. *Mol. Biol. Cell* **19**, 1485-1498.